AIAA JOURNAL
Vol. 40, No. 2, February 2002

Unsteady Flow Evolution in Porous Chamber with Surface Mass Injection, Part 2: Acoustic Excitation

Sourabh Apte* and Vigor Yang†
Pennsylvania State University, University Park, Pennsylvania 16802

Our earlier work on injection-driven flows in a porous chamber is extended to explore the effect of forced periodic excitations on the unsteady flowfield. Time-resolved simulations are performed to investigate the effects of traveling acoustic waves on large-scale turbulent structures for various amplitudes and frequencies of imposed excitations. The resultant oscillatory flowfield is decomposed into mean, periodic (or organized), and turbulent (or random) motions using a time-frequency localization technique. Emphasis is placed on the interactions among the three components of the flowfield. The primary mechanism for the transfer of energy from the mean to the turbulent motion is provided by the nonlinear correlations among the velocity fluctuations, as observed in stationary turbulent flows. The unsteady, deterministic component gives rise to an additional mechanism for energy exchange between the organized and turbulent motions and, consequently, produces increased turbulence levels at certain acoustic frequencies. The periodic excitations lead to earlier laminar-to-turbulence transition than that observed in stationary flows. The turbulence-enhanced momentum transport, on the other hand, leads to increased eddy viscosity and tends to dissipate the vortical wave originating from the injection surface. The coupling between the turbulent and acoustic motions results in significant changes in the unsteady flow evolution in a porous chamber.

Nomenclature

a = speed of sound
f = frequency, Hz
h = chamber half-height, m
I = turbulence intensity, $\sqrt{(\overline{u'u'} + \overline{v'v'})}$
L = chamber length, m
M_c = mean Mach number at centerline
M_{cr} = critical acoustic Mach number
M_{inj} = injection Mach number
$\dot{m}_w$ = injection mass flow rate, kg/m^{2}s
p = pressure, Pa
Re = Reynolds number
T = temperature, K
t = time, s
u = axial velocity, m/s
$\boldsymbol{u}$ = velocity vector
v = vertical velocity, m/s
v_w = injection velocity, m/s
γ = ratio of specific heats
δ = thickness of acoustic boundary layer
ε = magnitude of imposed periodic excitation
μ = dynamic viscosity, kg/ms
ν = kinematic viscosity, m^2/s
ν_t = turbulent eddy viscosity, m^2/s
ρ = density, kg/m^3
σ = shear stresss, kg/m^{2}s
τ = period of acoustic oscillation, s
φ = velocity potential
ψ = solenoidal velocity
$\boldsymbol{\Omega}$ = vorticity

Subscripts

b = bulk mean quantity
c = centerline
lam = laminar
w = wall

Superscripts

a = deterministic unsteady component
$'$ = fluctuating component due to turbulence

Averaging

$\bar{}$ = time-averaged quantity
$\leftrightarrow$ = density-weighted, time-averaged quantity
$\langle\,\rangle$ = ensemble averaging

I. Introduction

THE present work extends our previous study[1] on unsteady flow evolution in a porous chamber with surface mass injection, to include periodic excitations of the stationary flowfield. Traveling acoustic waves are obtained by imposing temporal oscillations at the head end of the chamber, with amplitudes and frequencies relevant to the intrinsic hydrodynamic flow instability. A time-resolved, large-eddy-simulation (LES) technique is used to compute the injection driven flow as elucidated previously.[1] The interactions between the mean and oscillatory flowfields may enhance turbulence intensity and cause early laminar-to-turbulence transition at certain frequencies of imposed excitations. This phenomenon is of utmost importance in the exploration of nonequilibrium turbulence, acoustically induced flow instability, unsteady scalar transport, and turbulent coherent structures in nonstationary environments. The study of energy-exchange mechanisms among the mean, deterministic (or periodic), and turbulent motions may also improve the understanding of self-sustained unstable motions within combustion chambers.

Turbulent flows under imposed organized oscillations have been investigated in a variety of configurations, including channel flows, flat-plate boundary layers, piston-driven resonating tubes, and combustion chambers of rocket and airbreathing engines. As a first attempt, Lighthill[2] provided an analytical framework for studying the responses of laminar skin-friction and heat-transfer coefficients to small external perturbations in velocity. The work was extended for turbulent flows by Patel[3] and Cebeci[4] using mixing-length and eddy-viscosity formulations, respectively. Considerable effort was contributed by Schachenmann and Rockwell[5] and Simpson et al.[6] to the investigation of the growth of boundary layers with mean pressure gradients. In spite of the progress made so far, detailed

Received 22 January 2001; revision received 9 July 2001; accepted for publication 19 July 2001.

*Graduate Research Assistant, Department of Mechanical Engineering.
†Professor, Department of Mechanical Engineering; vigor@psu.edu. Associate Fellow AIAA.

insight into the temporal evolution of turbulence under forced excitations remains limited because of the intricate interactions among the various constituent flowfields involved. The lack of a unified data-deduction procedure that can be applied to different flow conditions poses another difficulty.

Transition to turbulence in an oscillatory pipe flow was investigated by Merkli and Thomann[7] and Eckmann and Grotberg.[8] Their experiments proposed that turbulence occurs in the form of periodic bursts followed by relaminarization; however, fully turbulent flow was not observed during the whole cycle. Stability analysis of the acoustic boundary layer, that is, Stokes layer, in a turbulent environment has indicated that transition to turbulence is a local event, provided that the boundary-layer thickness $\delta = \mathcal{O}[\sqrt{(\nu/2\pi f)}]$ is small compared with the characteristic dimensions, that is, pipe diameter. Under these conditions, turbulence transition is governed by the local Reynolds number based on δ, that is, $Re_\delta = u^a\sqrt{(2/\nu\omega)}$, where u^a is the amplitude of the oscillatory axial velocity, ν the kinematic viscosity, and ω the radian frequency of periodic motions.[7,8] Effects of oscillatory motion on turbulence and mean flow properties in a fully developed turbulent pipe flow were also studied by Tu and Ramaprian[9] and Tardu and Binder,[10] among others.

Recently, Brereton et al.[11] carried out a thorough investigation of the effects of external unsteadiness on a well-developed flat-plate turbulent boundary layer by imposing periodic fluctuations downstream. The interactions between the organized and turbulent flowfields were studied at different frequencies of imposed oscillations. Statistical descriptions and correlations among the fluctuating velocity components of turbulent motions were found to be equivalent for the cases with and without freestream unsteadiness over a broad range of frequency. In view of turbulence as a broadband phenomenon, excitation at a single frequency did not exert any noticeable effect on the time-averaged properties of motion. A comprehensive review of recent advances in the study of wall-bounded unsteady turbulent flows was performed by Brereton and Mankbadi.[12]

In contrast to the observations made by Brereton et al.[11] and Brereton and Mankbadi[12] for boundary layers, forced oscillations may cause resonance or other profound responses within confined cavities, such as combustion chambers of rocket and airbreathing engines. This gives an impetus to investigate injection-driven flows in porous chambers, mainly because the chamber is almost entirely closed and the internal processes tending to attenuate unsteady motions are weak. Under these situations, enhanced turbulence production due to forced periodic excitations may appear at certain longitudinal eigenmodes of the chamber and consequently cause large excursions of unsteady flow motions. To address this phenomenon, Beddini and Roberts[13] and Lee and Beddini[14] explored the turbularization of the acoustic boundary layer in channel flows with and without surface transpiration, by means of simplified analytical and numerical analyses based on second-order turbulence closure schemes. The effect of pseudoturbulence at the injection surface on flow development was also addressed. The results indicated that the critical acoustic Mach number, $M_{cr} \sim \sqrt{(f\nu)}/\bar{a}$, required for acoustically induced transition of turbulence decreases with increase in surface injection velocity and pseudoturbulence level. A detailed analysis of this phenomenon is, however, necessary to explore the behavior of turbulent motions under forced oscillatory conditions. The effects of turbulence-enhanced momentum transport on organized periodic motions and mean flowfield need to be addressed.

To explore these issues, the present work includes time-resolved simulations and analyses of unsteady flow evolution in porous chambers with surface transpiration under forced acoustic excitations. In subsequent sections, the flow configuration and boundary conditions representative of a nozzleless solid-propellant rocket motor are summarized. A comprehensive data-deduction methodology is developed to separate the mean, periodic, and turbulent quantities from the instantaneous flowfield. The decomposition scheme is then employed to achieve considerable insight into the energy exchange mechanism among the three different fields. Finally, the phenomena of acoustically induced turbulence and the effect of turbulence-enhanced momentum transfer on the shear wave produced at the injection surface are addressed for a variety of forcing amplitudes and frequencies.

II. Flow Configuration and Boundary Conditions

The physical configuration under investigation follows our previous work presented in Ref. 1, which consists of a porous chamber closed at the head end and connected to a divergent nozzle downstream. Air is injected through the porous surface at a total temperature of 260 K and a total pressure of 3.142 atm. The mean injection mass flow rate is $\bar{m}_w = 13$ kg/m^{2}s. White noise is introduced to the injection mass flux, with the magnitude of perturbation being 1% of its mean quantity. After a stationary flow is obtained, periodic oscillations are imposed at the head end as follows to simulate traveling acoustic waves in the chamber:

$$p^a = \varepsilon\bar{p}\sin(2\pi f t) \tag{1}$$

$$u^a = \bar{p}/(\bar{p}\bar{a}) \tag{2}$$

where the overbar denotes time-averaged quantities and superscript a indicates organized unsteady oscillation. Here, ε and $\bar{a}$ represent the percentage of the mean pressure and speed of sound, respectively. There is no phase difference between the pressure and velocity fluctuations for such a simple traveling acoustic wave. Temperature fluctuations are obtained according to the isentropic relationship with pressure:

$$T^a = \bar{T}(1 + p^a/\bar{p})^{(\gamma-1/\gamma)} - \bar{T} \tag{3}$$

The boundary conditions along the porous walls are specified using the method of characteristics described in Ref. 1. The total mass flow rate and specific internal energy are kept constant, and vertical injection is enforced. Note that the present simulation is based on the pseudoturbulence level of 1% of the mean mass flow rate, corresponding to the low pseudoturbulence case considered in Ref. 1 to minimize the effect of imposed white noise on turbulence transition. The outflow is supersonic and requires no specification of physical boundary conditions. The flow variables at the nozzle exit are, thus, extrapolated from the computational domain. Finally, flow symmetry is assumed at the centerline.

III. Decomposition of Flow Variables

Figure 1 shows a typical pressure-time history obtained from the present study, including the mean, periodic, and turbulent motions. The triple decomposition introduced by Hussain and Reynolds[15] for incompressible flows is extended to include compressibility effects using Favre-averaged (or density-weighted) ensemble- and time-averaging techniques given hereafter. These averaging techniques offer mathematical simplification and eliminate triple correlations between density and velocity fluctuations in compressible flows. Accordingly, the calculated flow property from LES, $\tilde{\mathfrak{I}}^r(\boldsymbol{x}, t)$, can be expressed as the sum of the density-weighted time-averaged, periodic, and turbulent quantities as follows:

$$\tilde{\mathfrak{I}}^r(\boldsymbol{x}, t) = \overleftrightarrow{\mathfrak{I}}(\boldsymbol{x}) + \mathfrak{I}^a(\boldsymbol{x}, t) + \mathfrak{I}'(\boldsymbol{x}, t) \tag{4}$$

where $\overleftrightarrow{\mathfrak{I}}(\boldsymbol{x})$ is the density-weighted long time average, starting from the instant t_0 at which steady fluctuations of flow properties are observed; $\mathfrak{I}^a(\boldsymbol{x}, t)$ is the density-weighted phase average that represents the periodically fluctuating or deterministic unsteady part; and $\mathfrak{I}'(\boldsymbol{x}, t)$ is the turbulent fluctuations. Note that the decomposition given by Eq. (4) is based on ensemble and time averages

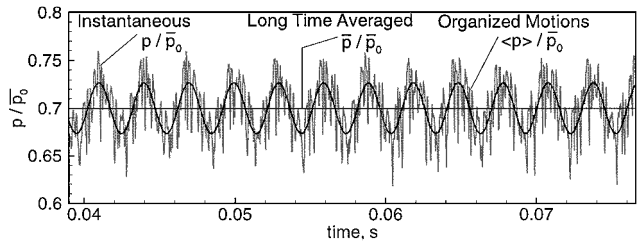

Fig. 1 Decomposition of unsteady flow property into mean, periodic, and turbulent quantities.

as opposed to the spatial filtering applied in Ref. 1 to obtain the unresolved, subgrid scales from turbulent motions. For clarity and simplicity, the superscript r and spatial filtering represented by the tilde are dropped on the right-hand side of Eq. (4). In summary, the flow variables obtained from the simulations in Ref. 1 are separated into three components as given here.

With time averaging,

$$\bar{\rho}\,\overleftrightarrow{\Im}(\boldsymbol{x}) = \overline{\rho\tilde{\Im}^r}$$

$$\overleftrightarrow{\Im}(\boldsymbol{x}) = \left[\lim_{N\to\infty}\frac{1}{N}\sum_{n=0}^{N-1}\rho\tilde{\Im}^r(\boldsymbol{x}, t_0 + n\Delta t)\right]\Bigg/\bar{\rho}$$

$$\text{where } N\Delta t \gg \tau \quad (5)$$

and with ensemble averaging,

$$\langle\rho\rangle[\overleftrightarrow{\Im}(\boldsymbol{x}) + \Im^a(\boldsymbol{x}, t)] = \langle\rho\tilde{\Im}^r(\boldsymbol{x}, t)\rangle$$

$$\langle\rho\tilde{\Im}^r(\boldsymbol{x}, t)\rangle = \lim_{N\to\infty}\frac{1}{N}\sum_{n=0}^{N-1}\rho\tilde{\Im}^r(\boldsymbol{x}, t + n\tau) \quad (6)$$

so that

$$[\rho\tilde{\Im}^r(x, t)]^a = \langle\rho\tilde{\Im}^r(x, t)\rangle - \overline{\rho\tilde{\Im}^r(x)} \quad (7)$$

where $\tau = 1/f$ is the period of forced oscillation and t_0 is the temporal location at which steady periodic motions are obtained.

Evaluation of the ensemble average given by Eq. (6) requires calculation and storage of flow quantities over a large number of cycles to achieve statistically consistent and meaningful results. To bypass this computational difficulty, time-frequency localization techniques based on wavelet or fast Fourier transform (FFT) theories can be used. The latter is employed in the present work. The fluctuating part, comprising turbulent and periodic oscillations, is first obtained by subtracting the long time averaged quantity from its instantaneous value. The FFT of these signals is computed to transform the data from the physical to the spectral space. The periodic signal is of known frequency and can be separated from the original signal by using a windowed Fourier transform (WFT) in the frequency domain. This extensive data-deduction technique, although straightforward, is very time consuming and is employed to obtain vertical variations of flow properties at selected axial locations. Details of this methodology are given in Refs. 16 and 17. The intercomponent energy transfer mechanisms can be studied by applying the aforementioned methodology to compute the mean, periodic, and turbulent flowfields within the chamber.

IV. Energy Transfer Among Mean, Deterministic, and Turbulent Flowfields

The equations of motion for an organized, unsteady, compressible flow are formulated by applying the decomposition procedure described in the preceding section to the conservation laws of mass and momentum.[16] The present work extends the analysis of Brereton et al.[11] for incompressible flows to accommodate the effect of fluid compressibility using density-weighted Favre averaging. Note that the following equations present a guideline to investigate the energy transport mechanisms in the presence of periodic oscillations. The simulations performed solve the Favre-filtered conservation equations of mass, momentum, and energy for the resolved scales of the motion with appropriate subgrid-scale models as described in Ref. 1. The continuity and momentum equations can be written in the following conservation form[16]:

$$\frac{\partial\rho}{\partial t} + \frac{\partial(\rho u_\ell)}{\partial x_\ell} = 0 \quad (8)$$

$$\frac{\partial(\rho u_k)}{\partial t} + \frac{\partial(\rho u_k u_\ell)}{\partial x_\ell} = -\frac{\partial\rho}{\partial x_k} + \frac{\partial\sigma_{k\ell}}{\partial x_\ell} \quad (9)$$

where viscous stresses are given as

$$\sigma_{kl} = -\frac{2}{3}\mu\frac{\partial u_j}{\partial x_j}\delta_{k\ell} + \mu\left(\frac{\partial u_k}{\partial x_\ell} + \frac{\partial u_\ell}{\partial x_k}\right) \quad (10)$$

By substituting Eq. (4) into Eq. (8) and making use of the definitions given in Eqs. (5–7), the continuity equations for the mean, deterministic (or organized), and turbulent flowfields are obtained:

$$\frac{\partial\bar{\rho}}{\partial t} + \frac{\partial(\bar{\rho}\overleftrightarrow{u}_\ell)}{\partial x_\ell} = 0 \quad (11)$$

$$\frac{\partial\rho^a}{\partial t} + \frac{\partial\left(\langle\rho\rangle u_\ell^a + \rho^a\overleftrightarrow{u}_\ell\right)}{\partial x_\ell} = 0 \quad (12)$$

$$\frac{\partial\rho'}{\partial t} + \frac{\partial(\langle\rho\rangle u'_\ell + \rho' u_\ell)}{\partial x_\ell} = 0 \quad (13)$$

Only the velocity components are averaged with density weighting to avoid correlations between density and velocity fluctuations in the momentum equations. The stresses and pressure are decomposed into the periodic, time-averaged, and random fluctuations according to the concept of Favre averaging to simplify these equations. When the ensemble averaging defined in Eqs. (6–9) is applied, the momentum equation for the periodically oscillatory flowfield becomes

$$\frac{\partial\langle\rho u_k\rangle}{\partial t} + \frac{\partial}{\partial x_\ell}\left[\langle\rho\rangle\left(\langle\overleftrightarrow{u}_k\overleftrightarrow{u}_\ell\rangle + \left\langle\overleftrightarrow{u}_k u_\ell^a\right\rangle + \left\langle u_k^a\overleftrightarrow{u}_\ell\right\rangle + \left\langle u_k^a u_\ell^a\right\rangle + \langle u'_k u'_\ell\rangle\right)\right]$$
$$= -\frac{\partial(\bar{p} + p^a)}{\partial x_k} + \frac{\partial\left(\overleftrightarrow{\sigma}_{k\ell} + \sigma_{k\ell}^a\right)}{\partial x_\ell} \quad (14)$$

The momentum equation for the mean flowfield can be obtained by taking the density-weighted long time average of either Eq. (9) or Eq. (14):

$$\frac{\partial(\bar{\rho}\overleftrightarrow{u}_k\overleftrightarrow{u}_\ell)}{\partial x_\ell} + \frac{\partial\left(\bar{\rho}\overleftrightarrow{u_k^a u_\ell^a}\right)}{\partial x_\ell} + \frac{\partial(\bar{\rho}\overleftrightarrow{u'_k u'_\ell})}{\partial x_\ell} = -\frac{\partial\bar{p}}{\partial x_k} + \frac{\partial(\overleftrightarrow{\sigma}_{k\ell})}{\partial x_\ell} \quad (15)$$

To deduce the momentum equation for turbulent fluctuations, Eq. (14) is subtracted from Eq. (9). Using the definitions of time- and ensemble-averaging, Eqs. (5) and (6), and noting that $(\,)^a \equiv \langle\,\rangle - \overleftrightarrow{(\,)}$, we have

$$\frac{\partial(\rho u'_k + \rho'\langle u_k\rangle)}{\partial t} + \frac{\partial}{\partial x_\ell}\left[\rho\left(\overleftrightarrow{u}_k u'_\ell + u_k^a u'_\ell + u'_k u_\ell^a + u'_k\overleftrightarrow{u}_\ell + u'_k u'_\ell\right)\right]$$
$$+ \frac{\partial}{\partial x_\ell}\left[\rho'\left(\overleftrightarrow{u}_k\overleftrightarrow{u}_\ell + \overleftrightarrow{u}_k u_\ell^a + u_k^a\overleftrightarrow{u}_\ell + u_k^a u_\ell^a + u'_k u'_\ell\right)\right]$$
$$= -\frac{\partial(p')}{\partial x_k} + \frac{\partial(\sigma'_{k\ell})}{\partial x_\ell} \quad (16)$$

The equations for kinetic energies in the mean, periodic, and turbulent flowfields can be derived from the preceding governing equations, and they provide a clearer interpretation of the relationship among the various flowfields in terms of measurable quantities.

A. Kinetic Energy of Mean Flowfield

The equation for $\overleftrightarrow{u}_\alpha\overleftrightarrow{u}_\alpha$ is formed by multiplying Eq. (15) by $\overleftrightarrow{u}_\alpha$, with $k = \alpha$. Rearranging the result and using the mean continuity equation (11), we have

$$\frac{\partial}{\partial x_\ell}\left(\bar{\rho}\overleftrightarrow{u}_\ell\frac{\overleftrightarrow{u}_\alpha\overleftrightarrow{u}_\alpha}{2}\right) = -\overleftrightarrow{u}_\alpha\frac{\partial\bar{p}}{\partial x_\alpha} - \frac{\partial}{\partial x_\ell}\left(\bar{\rho}\overleftrightarrow{u}_\alpha\overleftrightarrow{u_\alpha^a u_\ell^a} + \bar{\rho}\overleftrightarrow{u}_\alpha\overleftrightarrow{u'_\alpha u'_\ell}\right)$$
$$+ \overleftrightarrow{u}_\alpha\frac{\partial\overleftrightarrow{\sigma}_{\alpha\ell}}{\partial x_\ell} + \bar{\rho}\overleftrightarrow{u'_\ell u'_\alpha}\frac{\partial\overleftrightarrow{u}_\alpha}{\partial x_\ell} + \bar{\rho}\overleftrightarrow{u_\ell^a u_\alpha^a}\frac{\partial\overleftrightarrow{u}_\alpha}{\partial x_\ell} \quad (17)$$

B. Kinetic Energy of Periodic Flowfield

The equation for $\overleftrightarrow{u_\alpha^a u_\alpha^a}$ is similarly derived by subtracting Eq. (15) from Eq. (14) and multiplying the result by u_α^a, with $k = \alpha$. Taking the time average and making use of Eq. (12), we have

$$\frac{\partial}{\partial t}\left(\langle\rho\rangle\overleftrightarrow{\frac{u_\alpha^a u_\alpha^a}{2}}\right)+\frac{\partial}{\partial x_\ell}\left(\langle\rho\rangle\,\overleftrightarrow{u_\ell^a\frac{u_\alpha^a u_\alpha^a}{2}}\right)+\frac{\partial}{\partial x_\ell}\left(\langle\rho\rangle\ddot{u}_\ell\overleftrightarrow{\frac{u_\alpha^a u_\alpha^a}{2}}\right)$$

$$=-\overline{u_\alpha^a\frac{\partial p^a}{\partial x_a}}-\frac{\partial}{\partial x_\ell}\left(\langle\rho\rangle\,\overleftrightarrow{u_\alpha^a u_\ell' u_\alpha'}\right)+\overline{u_\alpha^a\frac{\partial\sigma_{\alpha\ell}^a}{\partial x_\ell}}+\langle\rho\rangle\,\overleftrightarrow{u_\ell' u_\alpha'}\frac{\partial u_\alpha^a}{\partial x_\ell}$$

$$-\langle\rho\rangle\overleftrightarrow{u_\ell^a u_\alpha^a}\frac{\partial\ddot{u}_\alpha}{\partial x_\ell}-\ddot{u}_\ell\overleftrightarrow{\rho^a u_\alpha^a}\frac{\partial\ddot{u}_\alpha}{\partial x_\ell}\tag{18}$$

Note that

$$\langle\rho\rangle\overleftrightarrow{u_\ell' u_\alpha'}\frac{\partial\ddot{u}_\alpha}{\partial x_\ell}$$

can be rearranged to give terms with time mean and periodic fluctuations in density:

$$\bar{\rho}\overleftrightarrow{u_\ell' u_\alpha'}\frac{\partial\ddot{u}_\alpha}{\partial x_\ell}+\overline{\rho^a u_\ell' u_\alpha'}\frac{\partial\ddot{u}_\alpha}{\partial x_\ell}$$

C. Kinetic Energy of Turbulent Flowfield

Similarly, multiplying Eq. (16) by u_α', with $k=\alpha$, and taking the time average, we have

$$\frac{\partial}{\partial t}\left(\bar{\rho}\overleftrightarrow{\frac{u_\alpha' u_\alpha'}{2}}\right)+\frac{\partial}{\partial x_\ell}\left(\bar{\rho}\ddot{u}_\ell\overleftrightarrow{\frac{u_\alpha' u_\alpha'}{2}}\right)+\frac{\partial}{\partial x_\ell}\left(\bar{\rho}\,\overleftrightarrow{u_\ell'\frac{u_\alpha' u_\alpha'}{2}}\right)$$

$$+\frac{\partial}{\partial x_\ell}\left(\bar{\rho}\,\overleftrightarrow{u_\ell'\frac{u_\alpha' u_\alpha'}{2}}\right)=-\overline{u_\alpha'\frac{\partial p'}{\partial x_\alpha}}+\overline{u_\alpha'\frac{\partial\sigma_{\alpha\ell}'}{\partial x_\ell}}-\bar{\rho}\,\overleftrightarrow{u_\ell' u_\alpha'}\frac{\partial u_\alpha^a}{\partial x_\ell}$$

$$-\bar{\rho}\overleftrightarrow{u_\ell' u_\alpha'}\frac{\partial\ddot{u}_\alpha}{\partial x_\ell}+\overline{\rho' u_k'\langle u_\ell\rangle}\frac{\partial\langle u_k\rangle}{\partial x_\ell}\tag{19}$$

In Eq. (19), the fourth-order correlation term between density and velocity fluctuations is neglected. Each of the time-averaged equations for the mean, periodic, and turbulent flow energies contain the convection, dissipation, production, and viscous and pressure diffusion terms. The production terms are of particular interest in understanding the energy exchange among the three constituent flowfields. Several important points are noted here.

First, the term

$$\bar{\rho}\overleftrightarrow{u_\ell' u_\alpha'}\frac{\partial\ddot{u}_\alpha}{\partial x_\ell}$$

appears, with opposite signs, in both Eqs. (17) and (19). It serves as a pathway to exchange the energy between the mean and turbulent fields. This term represents the primary production mechanism, as is also observed in stationary flows.

Second, the term

$$\bar{\rho}\overleftrightarrow{u_\ell^a u_\alpha^a}\frac{\partial\ddot{u}_\alpha}{\partial x_\ell}$$

which appears in both Eqs. (17) and (18), but with opposite signs, represents the product of the mean shear and the mean correlation between components of the deterministic velocity. It characterizes the energy transfer between the mean and deterministic fields and serves as a basis for explaining the phenomena of flow-turning loss and acoustic streaming.[18] The former refers to the loss of acoustic energy to the mean flow due to the misalignment between the acoustic and mean flow velocities. The latter describes the modification of the mean flowfield due to impressed periodic excitations.

Finally, kinetic energy is exchanged between the deterministic and turbulent fields, as characterized by the term

$$\bar{\rho}\,\overleftrightarrow{u_\ell' u_\alpha'}\frac{\partial u_\alpha^a}{\partial x_\ell}$$

which appears in both Eqs. (18) and (19). Its negative sign in Eq. (19) represents the production of turbulent kinetic energy due to periodic motions. Its positive sign in Eq. (18) represents a sink for the kinetic energy of periodic motions. The behavior of these three production terms in Eqs. (17–19) may help explain, in a time-averaged sense, the relationship among the mean, organized, and turbulent motions.

V. Results and Discussion

The effects of traveling acoustic waves on unsteady flow evolution were investigated in depth at several frequencies (i.e., 336, 676, 1000, 1346, 1500, and 1800 Hz) relevant to the intrinsic acoustic and hydrodynamic flow instabilities in the chamber. The excitation frequency of 336 Hz is roughly estimated to be to the first longitudinal acoustic mode of the porous chamber, based on the chamber length and speed of sound in the head-end region. The frequency of 1800 Hz, on the other hand, is close to the dominant frequency of the vortex shedding from the injection surface.[1] The nominal amplitude of pressure excitation ε was set to be 5% of the mean chamber pressure at the head end. The amplitude of $\varepsilon=2.5\%$ was also imposed at 336 Hz to study the effect of forcing amplitude on flow development. Statistically meaningful data were obtained after 10 cycles of oscillations were completed. The flow properties were then stored for 12 cycles for accurate analysis of the interactions among the mean, periodic, and turbulent flowfields.

A. Instantaneous Flowfield

Figure 2 shows the time evolution of the fluctuating pressure field within one cycle of oscillation at $f=336$ Hz, normalized by the mean chamber pressure at the head end. The oscillation amplitude ε is 5%. Only the upper half of the chamber is shown, with $y/h=1$ corresponding to the injection surface and $y/h=0$ to the centerline. The cyclic variation of the pressure field clearly indicates a planar acoustic wave traveling in the axial direction. The large pressure fluctuation in the downstream region may be attributed to the fluid compressibility effect at high Mach numbers and concentrated vortices surrounded by large-scale turbulent motions. The flowfield is basically characterized by a balance between the axial pressure gradient and inertia forces, as elucidated in Ref. 1.

Figure 3 shows the corresponding evolution of the fluctuating vorticity field. Oscillatory vorticity (also known as shear wave) arises from the injection surface because of the viscoacoustic interaction in the unsteady flowfield.[19,20] A slip flow associated with the irrotational acoustic motion is not allowed at the surface; the flow must enter the chamber in the radially inward direction with no axial component. This process inevitably produces vorticity, which is then convected downstream and dissipated by viscous effects. The acoustically induced shear waves undergo transition in the midsection of the motor, giving rise to turbulent motions. The large-scale structures in the acoustic environment appear to be more organized, compared with the case without acoustic waves, and exhibit strong interactions between turbulence and periodic excitations. Flandro[19] and Flandro et al.[20] established an analytical model dealing with the vorticity generation and transport in rocket motors with acoustic excitations. The velocity field $\boldsymbol{u}$ is decomposed into a solenoidal ψ

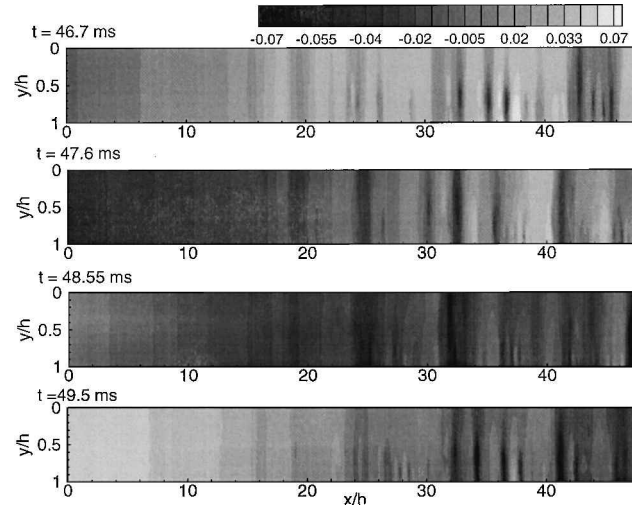

Fig. 2 Time evolution of fluctuating pressure field within one cycle of oscillation ($f=336$ Hz and $\varepsilon=5\%$).

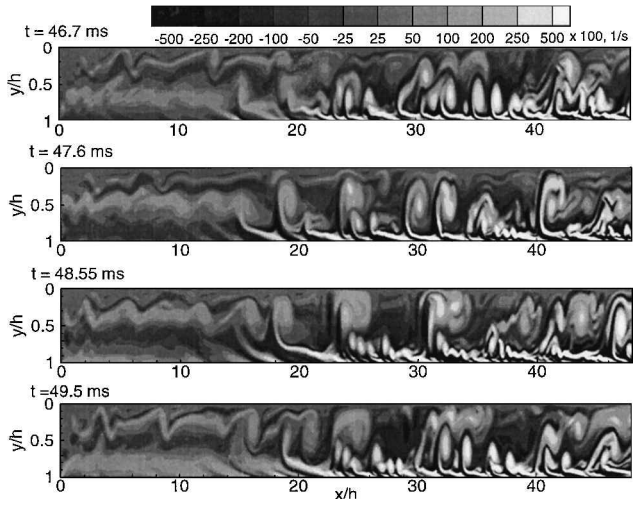

Fig. 3 Time evolution of fluctuating vorticity field within one cycle of oscillation ($f = 336$ Hz and $\varepsilon = 5\%$).

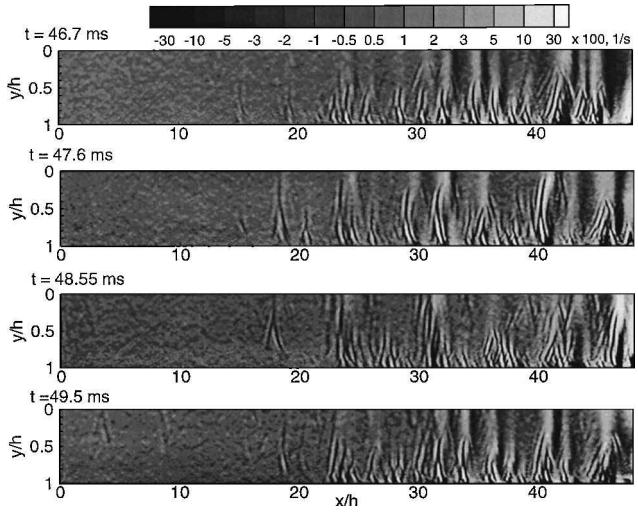

Fig. 4 Time evolution of fluctuating dilatation field within one cycle of oscillation ($f = 336$ Hz and $\varepsilon = 5\%$).

and a potential component φ as follows:

$$\boldsymbol{u} = \boldsymbol{\psi} + \nabla\varphi \tag{20}$$

The solenoidal field satisfies the incompressible condition:

$$\nabla \cdot \boldsymbol{\psi} = 0 \tag{21}$$

The vorticity field $\boldsymbol{\Omega}$ can be obtained from

$$\boldsymbol{\Omega} = \nabla \times \boldsymbol{u} = \nabla \times \boldsymbol{\psi} \tag{22}$$

Whereas the solenoidal field contains all of the vorticity in a given velocity field, the potential field φ includes all of the volume dilatation, such that

$$\nabla^2\varphi = \nabla \cdot \boldsymbol{u} = \Delta \tag{23}$$

where Δ denotes the dilatation field, which corresponds to the irrotational velocity field and characterizes density variations attributed to fluid compressiblity. The fluctuating dilatation field can be obtained by subtracting the time-averaged part from Eq. (23) and is shown in Fig. 4. Regions corresponding to the fluctuating pressure and concentrated high vorticity are clearly seen in the downstream region. The acoustic velocity potential is small in the upstream region, where the flow is nearly incompressible and laminar. The dilatation field and its associated acoustic velocity potential, however, are significantly influenced by the turbulence-enhanced momentum transport and compressibility effects in the downstream region.

The effect of excitation frequency on the unsteady flowfield evolution is addressed. Figure 5 shows snapshots of the fluctuating vorticity fields for different forcing frequencies. For low frequencies, for example, 336 and 1000 Hz, turbulence transition is initiated earlier in the upstream region, as compared with the case without acoustic excitations.[1] This indicates that low-frequency oscillations tend to promote the energy exchange among the mean, periodic, and turbulent flowfields and, consequently, lead to enhanced turbulence levels in the upstream region. In particular, highly organized vortical structures are observed in the midsection of the motor at $f = 1000$ Hz. For higher frequencies, for example, 1346 and 1800 Hz, however, transition to turbulence is delayed to a downstream location. The turbulence intensity in the upstream region is minimal, as evidenced by the layered structure of the laminar shear wave that results from the enforcement of the no-slip condition at the injection surface in an acoustic wave environment. Figure 5 also indicates that the size of these vortical structures changes with frequency. A simple scaling estimate of the acoustic boundary-layer thickness, that is, the Stokesian thickness, gives $\delta = \sqrt{(\nu/f)}$ for a laminar flow. For higher frequencies, δ is smaller and viscous stresses become so high as to prevent early initiation of turbulence. The acoustic motions at lower frequencies, on the other hand, exert a more significant influence on the oscillatory flowfield and, thus, facilitate energy transfer among the three components of the velocity field.

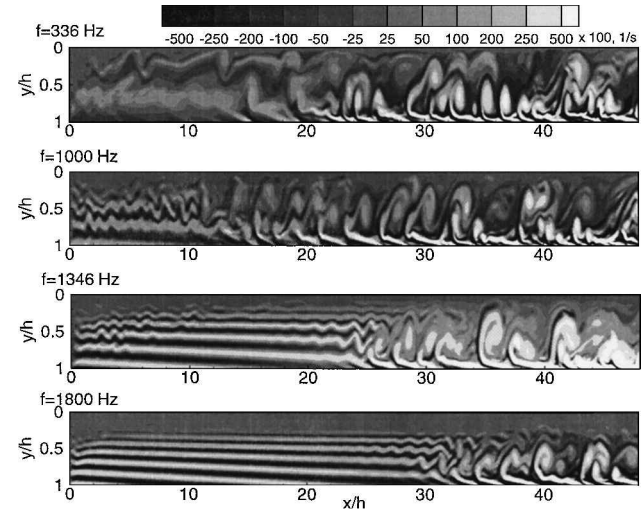

Fig. 5 Snapshots of fluctuating vorticity fields at different frequencies of forced excitations ($\varepsilon = 5\%$).

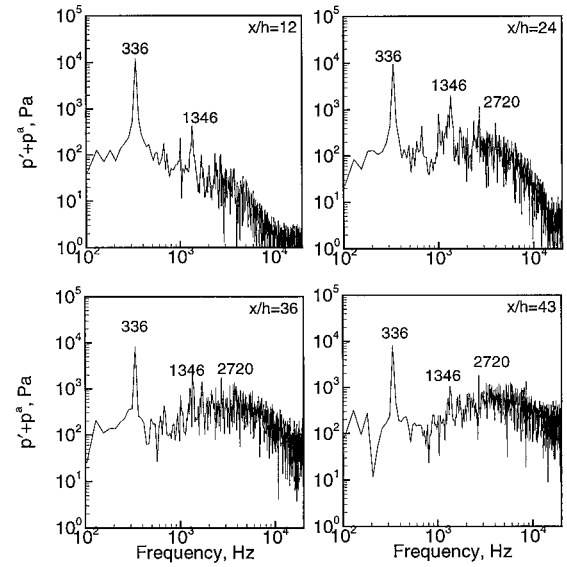

Fig. 6 Power spectral density of pressure fluctuations at various axial locations ($f = 336$ Hz and $\varepsilon = 5\%$), $y/h = 0.9$.

Figures 6 and 7 show the power spectral densities of pressure and axial velocity fluctuations at various axial locations for

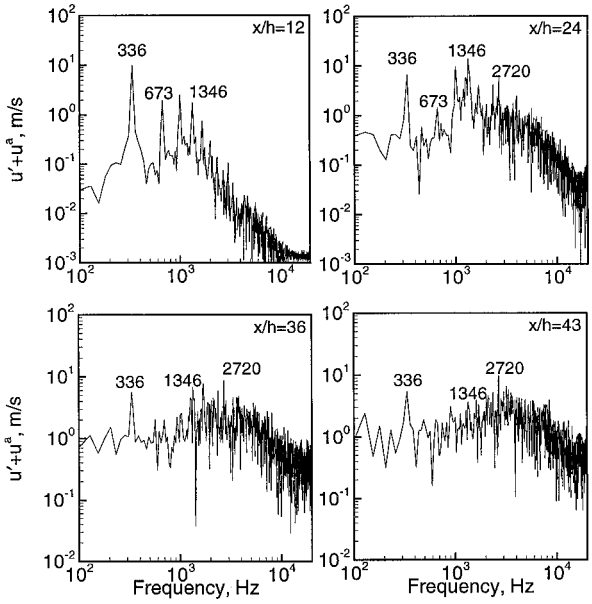

Fig. 7 Power spectral density of axial velocity fluctuations at various axial locations ($f = 336$ Hz and $\varepsilon = 5\%$); $y/h = 0.9$.

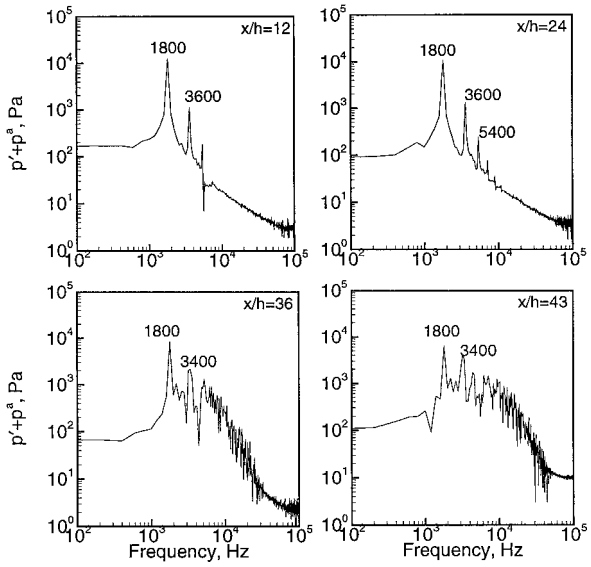

Fig. 8 Power spectral density of pressure fluctuations at various axial locations ($f = 1800$ Hz and $\varepsilon = 5\%$); $y/h = 0.9$.

$f = 336$ Hz and $\varepsilon = 5\%$, respectively. All of the measurements are taken at a vertical location of $y/h = 0.9$. The corresponding plots for $f = 1800$ Hz are shown in Figs. 8 and 9 for comparison. Several points should be noted here. First, for low-frequency forced oscillations, broadband fluctuations in pressure and axial velocity are observed even in the upstream region, which indicates early transition to turbulence. Second, the peak magnitude at the impressed frequency decreases in the downstream region, mainly due to the flow-turning loss in the chamber as discussed hereafter. Third, at higher forcing frequencies, the spectra for pressure and velocity fluctuations appear significantly different in the upstream region than their low-frequency counterparts. The broadband turbulence spectra observed in the upstream region for lower excitation frequencies are absent. Instead, organized motions are triggered at integer multiples of the impressed frequency, and the flow becomes turbulent farther downstream. Finally, the effects of impressed oscillations on the power density spectra are noted. The peaks in these spectra change according to the frequencies of impressed oscillations, indicating modification of the large-scale motions in the downstream region compared with the case without acoustic excitations. This phenomenon is also evidenced in the photographs of the fluctuating vorticity fields shown in Fig. 5.

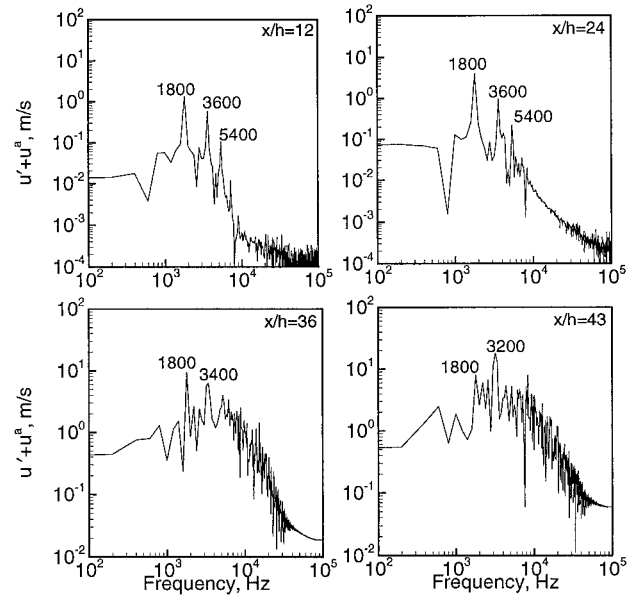

Fig. 9 Power spectral density of axial velocity fluctuations at various axial locations ($f = 1800$ Hz and $\varepsilon = 5\%$); $y/h = 0.9$.

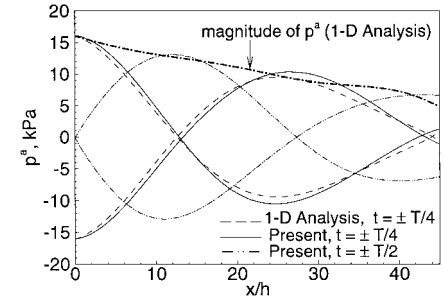

Fig. 10 Temporal evolution of axial distribution of acoustic pressure ($f = 336$ Hz and $\varepsilon = 5\%$).

The preceding observations suggest that the complex interactions among the periodic and turbulent motions are highly frequency dependent. As indicated in Eqs. (18) and (19), the term $\bar{\rho}\,\overleftrightarrow{u'_\ell u'_\alpha}\,\partial u^a_\alpha/\partial x_\ell$ appears as a source term in the turbulence energy equation but as a sink term in the kinetic energy equation for deterministic unsteady fluctuations. The periodic motions feed energy to the turbulent flowfield and lead to early transition in the low-frequency regime.

B. Interactions Between Mean and Acoustic Flowfields

The axial variation of the acoustic pressure field can be estimated using an approximate analysis that accounts for planar traveling wave propagation in an injection-driven channel flow.[16,17] The quasi-one-dimensional acoustic field in the chamber is formulated by applying the conservation laws to an infinitesimal control volume enclosing the flow passage at a given cross section. Culick's[21] and Culick and Yang's[22] one-dimensional model was extended to incorporate cross-sectional area variation and compressibility effects. A wave equation for the injection-driven flow is then derived and solved with appropriate boundary conditions.[17] Figure 10 shows the distributions of the acoustic pressure at four different times within one cycle of oscillation for $f = 336$ Hz and $\varepsilon = 5\%$. Excellent agreement with the analytical solution is obtained. The decrease in the magnitude of the pressure oscillation in the axial direction indicates the presence of flow-turning losses. The process takes place when a flow particle enters the chamber in a direction perpendicular to the porous surface and carries no kinetic energy contributed to the longitudinal waves. The particle then undergoes a turn into the direction parallel to the chamber axis and eventually participates in the periodic motion, mainly axial oscillations. During this process, the incoming flow acquires energy from the original acoustic field, representing a redistribution of acoustic energy. The one-dimensional model of Culick[21] and Culick and Yang[22] indicates that the acoustic

field loses its energy at a rate twice that obtained by the incoming flow. This loss can be regarded as the net exchange of energy from the acoustic field to the mean flowfield and is termed the flow-turning loss.

Hersh and Walker[23] conducted an experimental investigation into this phenomenon. They measured the variation of acoustic pressure along the centerline and the acoustic energy fluxes at two test sections, one upstream and one downstream. Baum and Levine[24] also used the acoustic energy flux to identify the flow-turning loss in their numerical analysis. If the amplitude of acoustic pressure decreases as the wave propagates, and the downstream energy flux is smaller than that upstream, flow-turning losses are present. The same concept is explored in the present simulations. Figure 10 shows a 35% decrease in acoustic pressure between the head end and the chamber exit. This indicates a large amount of flow-turning losses in the flowfield that may be attributed to the high crossflow speed and compressibility effect. The situation is quite different from those studied by Flandro,[19] in which the injection velocity is much smaller.

The effect of periodic motion on the mean flowfield, termed acoustic streaming, is also investigated.[18] The modification of the mean flowfield through acoustically induced turbulence is found to be minimal. The kinetic energy of periodic motion, however, decreases from the head end toward the nozzle region, a situation that can be attributed to the turbulence effects and flow-turning losses present within the chamber.

C. Effect of Imposed Periodic Excitation on Turbulence Properties

The triple decomposition defined in Eq. (4) enables energy transfer to be viewed as taking place among the three participating fields. This modifies the definition of turbulence stress for a nonstationary flow as follows:

$$\tau_{kl} = -\overline{\rho u_k' u_l'} - \overline{\rho u_k^a u_l^a} \tag{24}$$

It differs from its form for a stationary flow by virtue of an additional stress due to the organized part of unsteady motion, $-\overline{\rho u_k^a u_l^a}$. A set of differential equations describing the transport of the variance of the turbulent and periodic axial velocities is deduced in the component form, that is, Eqs. (18) and (19). The production of the axial component of turbulent kinetic energy, $\overleftrightarrow{\rho u'u'}$, includes $\overleftrightarrow{\bar{\rho}\, u'v'}\partial\tilde{u}/\partial y$ and $\overleftrightarrow{\bar{\rho}\, u'v'}\partial u^a/\partial y$. Whereas the former is equally important for stationary turbulence, the latter accounts for the energy exchange between the turbulent and periodic fields.

Figures 11 and 12 show the vertical distributions of the Reynolds stress, turbulence intensity, and periodic-flow (including both acoustic and organized shear waves) energy at various axial locations for

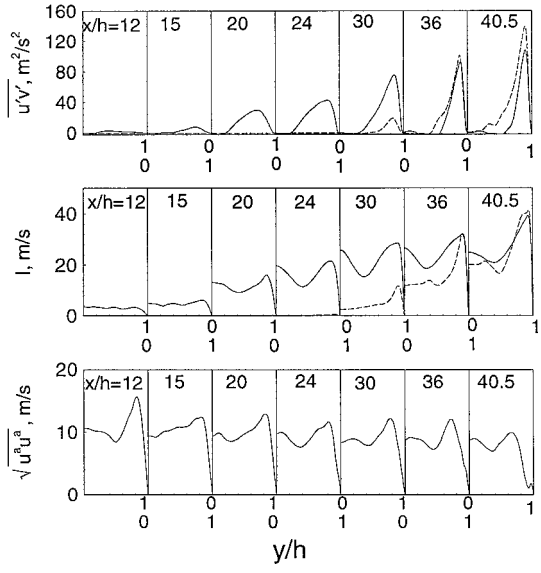

Fig. 11 Vertical distributions of Reynolds stress, turbulence intensity, and periodic-flow energy at various axial locations for $f = 336$ Hz and $\varepsilon = 5\%$: ----, without forced oscillation, and ——, with forced oscillation.

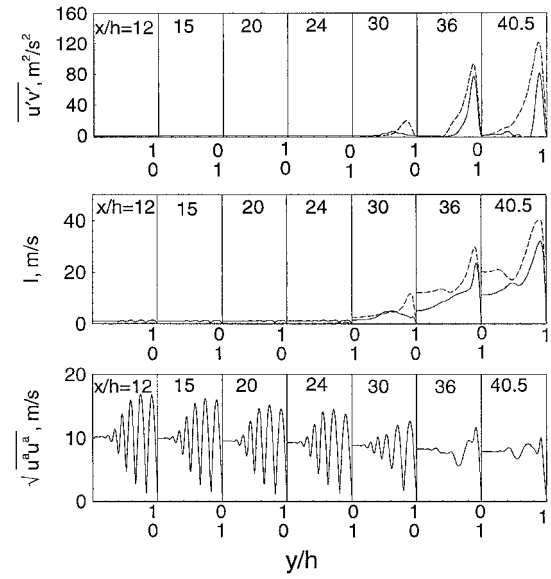

Fig. 12 Vertical distributions of Reynolds stress, turbulence intensity, and periodic-flow energy at various axial locations for $f = 1800$ Hz and $\varepsilon = 5\%$: ----, without forced oscillation and ——, with forced oscillation.

$f = 336$ and 1800 Hz, respectively. The corresponding properties for stationary flows are also indicated for comparison. The enhanced level of turbulence in the upstream region of the chamber at the low-frequency excitation ($f = 336$ Hz) represents transfer of energy from the acoustic to the turbulent field. The acoustic wave can indeed invoke hydrodynamic instability at low frequencies and initiate turbulence transition. Farther downstream, the intensity levels off to its value in the stationary flow case. The increased velocity gradient in the mean flow causes the effect of $\overleftrightarrow{\bar{\rho}\, u'v'}\partial\tilde{u}/\partial y$ to override the energy production arising from acoustic excitation. The turbulence intensity and stress level for the higher frequency case of $f = 1800$ Hz (Fig. 12), on the other hand, indicate limited change in the upstream region compared with the case without imposed excitation. With an increase in the forcing frequency, the acoustic boundary-layer thickness is reduced, and it exerts limited influence on turbulence production in the upstream region, due to the effectiveness of viscous dissipation.[19,20] Figures 11 and 12 also indicate the decreasing levels of periodic-flow energy in the downstream region due to the flow-turning losses discussed before. The acoustically induced vorticity is considerably damped in the upstream region for the low-frequency case, a phenomenon that can be attributed to the turbulence-produced eddy viscosity, which suppresses the shear wave arising from the injection surface.[20]

D. Effect of Turbulence on Periodic Motion

Although acoustic oscillations often enhance turbulence intensity through their interactions, turbulence tends to dissipate organized shear wave motion due to enhanced momentum transfer measured by the turbulent eddy viscosity,[20] obtained from the resolved scale length and time scales. Figure 13 shows four snapshots of the axial velocity fluctuation, including both turbulent and periodic components, for different excitation frequencies. The oscillatory velocity field exhibits a multidimensional structure. At higher frequencies, organized shear waves produced at the injection surface due to the no-slip condition are clearly observed in the upstream region. Turbulence fluctuations override periodic oscillations in the downstream region and damp out the shear waves.

Figures 14 and 15 present the vertical variations of the periodic axial velocity fluctuations u^a at various axial locations for $f = 673$ and 1346 Hz, respectively. To elucidate the effect of turbulence, results for pure laminar flows are also included, as denoted by the dashed lines. The velocity fluctuation in the core-flow region is governed by the isentropic relationship with the acoustic pressure, $u^a = p^a/\bar{\rho}\bar{a}$. In the upstream laminar regime, a velocity overshoot is observed near the porous wall because of the presence of the shear wave.[19] In the present study, the magnitude of the velocity

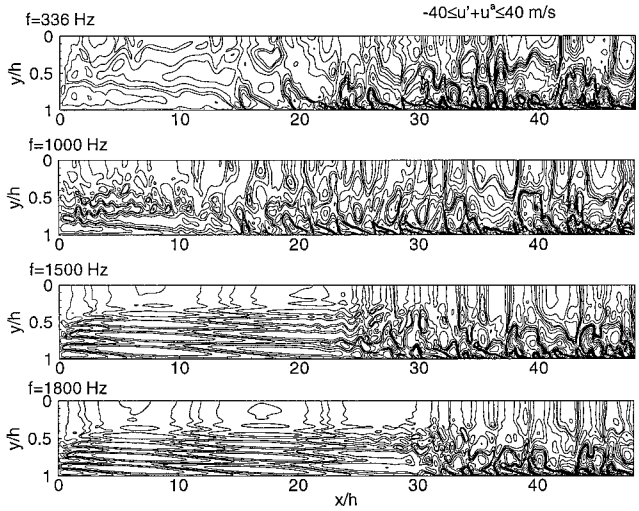

Fig. 13 Contour plots of fluctuating axial velocities at various excitation frequencies ($\varepsilon = 5\%$).

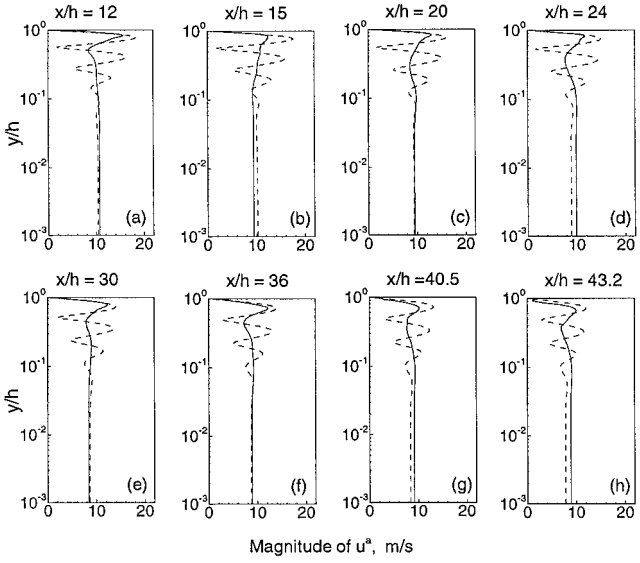

Fig. 14 Amplitudes of periodically fluctuating axial velocities at various axial locations for $f = 673$ Hz and $\varepsilon = 5\%$: - - - -, laminar flow and ——, turbulent flow.

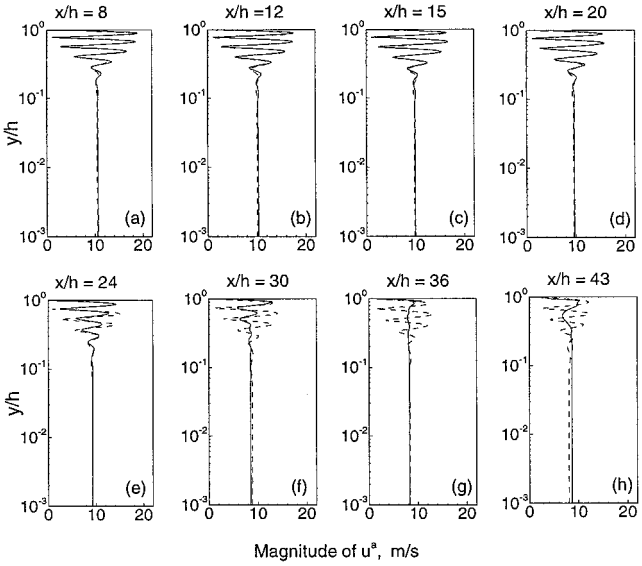

Fig. 15 Amplitudes of periodically fluctuating axial velocities at various axial locations for $f = 1346$ Hz and $\varepsilon = 5\%$: - - - -, laminar flow and ——, turbulent flow.

overshoot is smaller than twice the centerline fluctuating velocity, as predicted by Flandro[19] in his theoretical analysis. The high chamber pressure (around 100 atm) considered in his work gives rise to a very small surface injection velocity, and, hence, a prominent acoustic boundary layer is obtained. The strong blowing effect arising from the high injection velocity in the present work, however, extends the acoustic boundary layer and spreads the shear wave through the bulk of the chamber. This reduces the magnitude of the overshoot of the axial velocity fluctuation near the porous wall.

The shear wave travels toward the centerline with the mean vertical velocity and is damped out by viscous dissipation in the core-flow region. The shear stress σ^a_{lam} given by Eq. (10) is proportional to the rate at which the axial velocity changes in the vertical direction:

$$\sigma^a_{\text{lam}} \sim \frac{\partial u^a}{\partial y} \sim \frac{\Delta u^a}{\Delta y} \tag{25}$$

As the fluid element moves closer to the centerline, the number of reversals per unit radial distance traveled becomes much larger, mainly because of the diminished vertical velocity toward the centerline. This leads to increased shear stress and, consequently, damps the shear wave in the core region. The acoustic velocity amplitude divided by the distance traveled by the fluid particle in one-fourth of the acoustic period provides a reasonable estimate for the velocity gradient, as discussed by Flandro.[19] Thus, the shear stress near the wall becomes

$$\sigma^a_{\text{lam}} \sim 4f/M_{\text{inj}} \tag{26}$$

where M_{inj} is the mean-flow Mach number at the injection surface. Equation (26) indicates that, for high frequencies, the shear-stress levels become so important that viscous dissipation dominates the behavior of the oscillatory flowfield.

The periodic velocity fluctuation in the upstream region for $f = 673$ Hz is more suppressed than that at the higher frequency of 1346 Hz. This can be attributed to the acoustic wave-induced turbulence and its ensuing increase in the eddy viscosity ν_t in that region. Figure 16 shows the effect of turbulence on the magnitude and phase of axial velocity fluctuations in the midsection of the chamber ($x/h = 24$) for $f = 673$ Hz. The large turbulent eddy viscosity ν_t near the injection surface suggests efficient dissipation of the shear wave.

E. Acoustically Induced Turbulence Transition

In an effort to characterize acoustically induced turbulence, Beddini and Roberts[13] and Lee and Beddini[14] investigated channel flows with and without surface mass injection and defined a critical acoustic Mach number as the criterion for turbulence transition under periodic excitations. This number can be obtained by balancing the production and dissipation terms in the momentum equation for periodic oscillations, Eq. (18), with appropriate scaling:

$$M_{\text{cr}} = K\sqrt{f\nu}/\bar{a} \tag{27}$$

The constant K varies considerably, from 188 to 915, as indicated by Merkli and Thomann[7] for their experiments on flat-plate boundary layers with imposed freestream unsteadiness. In the present configuration with surface mass injection, the normalized surface injection velocity, $v_w/\sqrt{(\nu f)}$, is another important parameter determining the turbulence transition behavior. Beddini and Roberts[13] observed that the critical acoustic Mach number decreases with increasing injection velocity and pseudoturbulence level at the injection surface.

For the range of frequency studied in the present work, the critical acoustic Mach number is calibrated by observing turbulence transition for a given magnitude of imposed centerline acoustic velocity, $u^a_c = p^a/\bar{\rho}\bar{a}$. The amplitude of the pressure excitation at the head end is 5% of the mean chamber pressure, and the corresponding acoustic Mach number is $u^a_c/\bar{a} = 0.036$. By the use of Eq. (27) and by the observation of acoustically induced turbulence levels in the upstream region, the coefficient K attains a value of around 170. Note that occurrence of early transition to turbulence was inferred based on the evaluation of turbulence intensity at locations

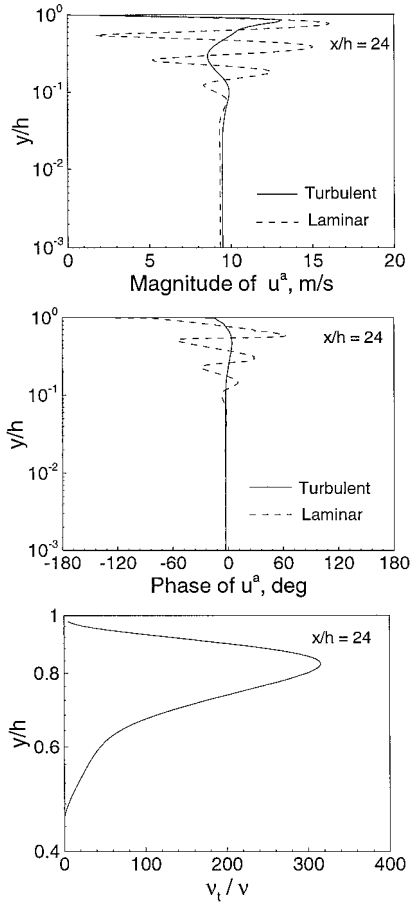

Fig. 16 Effect of turbulence on vertical variations of amplitude and phase of axial velocity fluctuation for $f = 673$ Hz and $\varepsilon = 5\%$; $x/h = 24$.

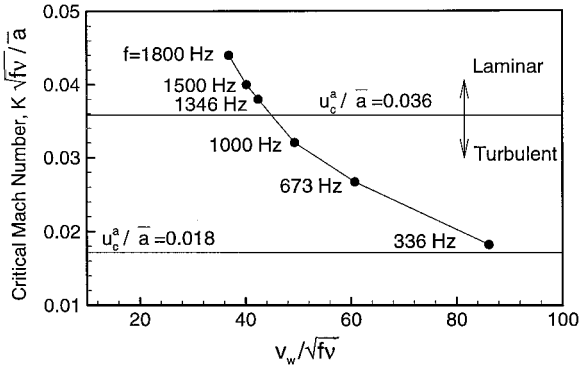

Fig. 17 Criterion for acoustically induced turbulence transition in porous chamber with surface mass injection.

upstream of $x/h = 30$, where turbulence transition occurred for the case without imposed excitations.

In the present study, the injection mass flow rate and the pseudoturbulence level were kept constant. The variation of the critical acoustic Mach number with normalized injection velocity was investigated using frequency as a parameter. The result is shown Fig. 17. With increased frequency, the normalized surface mass injection velocity decreases, and, as a result, the critical Mach number required for transition increases. Accordingly, early transition occurs for the frequencies of 336, 673, and 1000 Hz, and very limited enhancement of turbulence intensity in the upstream region is observed with periodic excitations at higher frequencies of 1346 and 1800 Hz.

The effect of the magnitude of imposed oscillation is also studied by reducing the forcing amplitude ε to 2.5% at 336 Hz. The corresponding acoustic Mach number at the centerline $u_c^a/\bar{a}$ shown in Fig. 17 is 0.018. As predicted by the present transition criterion, acoustically induced turbulence is minimal for this case and the flow

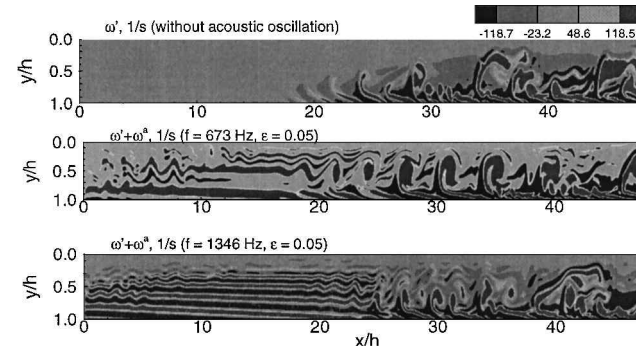

Fig. 18 Snapshots of fluctuating vorticity fields with and without externally imposed traveling acoustic waves at head end.

remains laminar in the upstream regime.[16] It should be cautioned that these computations lack the vortex-stretching mechanism present in three-dimensional flowfields, which may play an important role in redistributing the turbulence intensity and consequently modifying the interactions between acoustic and turbulent flowfields. A comprehensive three-dimensional simulation is necessary to corroborate and further refine the present findings.

F. Summary of Unsteady Flow Evolution Under Forced Periodic Oscillations

Figure 18 summarizes the evolution of the unsteady flows with and without external forcing. The imposed periodic excitations initiate early turbulence transition in the chamber in the low-frequency regime. The large vortical structures in the turbulent regime observed in the stationary flow case are significantly modified, depending on the magnitude and frequency of imposed oscillations. Several important points should be noted here. First, the unsteady flowfield can be decomposed into mean, periodically oscillatory, and turbulent motions. This triple decomposition can be used to explore the energy-exchange mechanisms among the three constituent flowfields. Acoustic waves generated by imposed oscillatory motion lead to enhanced turbulence levels in the upstream region at certain frequencies. Turbulence thus produced, on the other hand, suppresses the periodic shear wave generated at the injection surface due to enhanced momentum and energy transport. Second, the acoustically induced turbulence transition is highly frequency dependent. At higher frequencies, the viscous dissipation effect in the oscillatory flowfield becomes stronger, thereby suppressing early turbulence transition. Third, the mean flowfield is not significantly modified from its stationary-flow counterpart in the present study. The acoustic field, on the other hand, weakens from the head end toward the chamber exit owing to the flow-turning losses arising from the interactions between the mean and acoustic flowfields. Finally, the phenomenon of acoustically induced turbulence transition can be characterized by the critical acoustic Mach number and normalized injection velocity. With increases in injection velocity and surface-generated pseudoturbulence level, the critical acoustic Mach number required for transition decreases. Turbulent motion may be observed in the upstream region throughout the entire cycle of periodic oscillation only if the amplitude and frequency of the acoustic excitation meet certain requirements. Validation of these findings against experimental data is necessary.

VI. Conclusions

Time-resolved computations of injection driven flows in a porous chamber were performed based on the LES technique. Interactions among the mean, periodic, and turbulent motion were studied in detail by imposing traveling acoustic waves in a stationary flow. Several cases with different excitation frequencies and amplitudes of imposed pressure fluctuations were investigated. The mutual coupling between the turbulent and acoustic motions results in significant changes in the unsteady flow evolution in the chamber. The phenomenon of acoustically induced turbulence was observed when the forcing frequency falls below its critical value for a given amplitude of oscillation and pseudoturbulence level.

References

[1] Apte, S., and Yang, V., "Unsteady Flow Evolution in a Porous Chamber with Surface Mass Injection, Part 1: Free Oscillation," *AIAA Journal*, Vol. 39, No. 8, 2001, pp. 1577–1586.

[2] Lighthill, M. J., "The Response of Laminar Skin Friction and Heat Transfer to Fluctuations in the Stream Velocity," *Proceedings of the Royal Society of London, Series A: Mathematical and Physical Sciences*, Vol. 224, 1954, pp. 741–773.

[3] Patel, M. H., "On Turbulent Boundary Layers in Oscillatory Flow," *Proceedings of the Royal Society of London, Series A: Mathematical and Physical Sciences*, Vol. 353, 1977, pp. 121–144.

[4] Cebeci, T., "Calculation of Unsteady Two-Dimensional Laminar and Turbulent Boundary Layer to Random Fluctuations in External Velocity," *Proceedings of the Royal Society of London, Series A: Mathematical and Physical Sciences*, Vol. 335, 1977, pp. 225–238.

[5] Schachenmann, A. A., and Rockwell, D. O., "Oscillating Turbulent Flow in a Conical Diffuser," *Journal of Fluids Engineering*, Vol. 98, 1976, pp. 695–701.

[6] Simpson, R. L., Shivaprasad, B. G., and Chew, Y. T., "The Structure of a Separating Turbulent Boundary Layer, Part 4: Effects of Free-Stream Unsteadiness," *Journal of Fluid Mechanics*, Vol. 127, 1983, pp. 219–261.

[7] Merkli, P., and Thomann, H., "Transition to Turbulence in Oscillating Pipe Flow," *Journal of Fluid Mechanics*, Vol. 68, Pt. 3, 1975, pp. 567–575.

[8] Eckmann, D. M., and Grotberg, J. B., "Experiments on Transition to Turbulence in Oscillatory Pipe Flows," *Journal of Fluid Mechanics*, Vol. 222, 1991, pp. 329–350.

[9] Tu, S. W., and Ramaprian, B. R., "Fully Developed Periodic Turbulent Pipe Flow, Part 1: Main Experimental Results and Comparison with Predictions," *Journal of Fluid Mechanics*, Vol. 137, 1983, pp. 31–58.

[10] Tardu, S., and Binder, G., "Modulation of Bursting by Periodic Oscillations Imposed on Channel Flow," *Proceedings of Sixth Symposium on Turbulent Shear Flows*, 1987, pp. 4.5.1–4.5.6.

[11] Brereton, G., Reynolds, W., and Jayaraman, R., "Response of a Turbulent Boundary Layer to Sinusoidal Free-Stream Unsteadiness," *Journal of Fluid Mechanics*, Vol. 221, 1990, pp. 131–159.

[12] Brereton, G. J., and Mankbadi, R. R., "Review of Recent Advances in the Study of Unsteady Turbulent Internal Flows," *Applied Mechanics Review*, Vol. 48, No. 4, 1995, pp. 189–212.

[13] Beddini, R. A., and Roberts, T. A., "Turbularization of an Acoustic Boundary Layer on a Transpiring Surface," *AIAA Journal*, Vol. 26, No. 8, 1988, pp. 917–923.

[14] Lee, Y. H., and Beddini, R. A., "Acoustically Induced Turbulent Transition in Solid Propellant Rocket Chamber Flowfields," AIAA Paper 99-2508, 1999.

[15] Hussain, A. K. M. F., and Reynolds, W. C., "The Mechanics of Organized Wave in Turbulent Shear Flow," *Journal of Fluid Mechanics*, Vol. 41, 1970, pp. 241–258.

[16] Apte, S. V., "Unsteady Flow Evolution and Combustion Dynamics of Homogeneous Solid Propellant in a Rocket Motor," Ph.D. Dissertation, Dept. of Mechanical and Nuclear Engineering, Pennsylvania State Univ., University Park, PA, July 2000.

[17] Apte, S. V., and Yang, V., "Effects of Acoustic Oscillation on Flow Development in a Simulated Nozzleless Rocket Motor," *Solid Propellant Chemistry, Combustion, and Motor Interior Ballistics*, edited by V. Yang, T. B. Brill, and W. Z. Ren, Vol. 185, Progress in Aeronautics and Astronautics, AIAA, Reston, VA, 2000, Chap. 3.1, pp. 791–822.

[18] Tseng, I. S., "Numerical Simulation of Velocity-Coupled Combustion Response of Solid Rocket Propellants," Ph.D. Dissertation, Dept. of Mechanical Engineering, Pennsylvania State Univ., University Park, PA, 1992.

[19] Flandro, G. A., "Effects of Vorticity on Rocket Combustion Stability," *Journal of Propulsion and Power*, Vol. 11, No. 4, 1995, pp. 607–625.

[20] Flandro, G. A., Cai, W. D., and Yang, V., "Turbulent Transport in Rocket Motor Unsteady Flowfield," *Solid Propellant Chemistry, Combustion, and Motor Interior Ballistics*, edited by V. Yang, T. B. Brill, and W. Z. Ren, Vol. 185, Progress in Astronautics and Aeronautics, AIAA, Reston, VA, 2000, Chap. 3.3, pp. 837–858.

[21] Culick, F. E. C., "The Stability of One-Dimensional Motions in a Rocket Motor," *Combustion Science and Technology*, Vol. 7, 1973, pp. 165–175.

[22] Culick, F. E. C., and Yang, V., "Prediction of Stability of Unsteady Motions in Solid Propellant Rocket Motors," *Nonsteady Burning and Combustion Instability of Solid Propellants*, edited by L. DeLuca, E. W. Price, and M. Summerfield, Vol. 143, Progress in Astronautics and Aeronautics, AIAA, Washington, DC, 1992, Chap. 18, pp. 719–779.

[23] Hersch, A. S., and Walker, B., "Experimental Investigation of Rocket Motor Flow-Turning Acoustic Losses," U.S. Air Force Rocket Propulsion Lab., TR-84-009, Edwards AFB, CA, 1984.

[24] Baum, J. D., and Levine, J. N., "Numerical Study of Flow Turning Phenomenon," AIAA Paper 86-0533, 1986.

J. P. Gore
Associate Editor